POLITECNICO DI TORINO
Repository ISTITUZIONALE

Raman Broad Scans of Rare Earth Oxide (REO) Glasses from RRUFF Database, Compared to the Raman spectra of RE Oxides from Raman Open Database

(Article begins on next page)

19 September 2024

Raman Broad Scans of Rare Earth Oxide (REO) Glasses from RRUFF Database, Compared to the Raman spectra of RE Oxides from Raman Open Database

Amelia Carolina Sparavigna[1] ✎

[1]Department of Applied Science and Technology, Polytechnic University of Turin

RRUFF database is proposing the Raman broad scans of glasses $CaO-Al_2O_3-SiO_2$ with rare earth element (REE) oxides, that is of $CaO-RE_2O_3-Al_2O_3-SiO_2$ glasses. Raman data are courtesy of E. Cairns, University of Edinburgh. Here we show how we can use the q-BWF functions to decompose these spectra. The q-BWF functions are generalizing the Breit-Wigner-Fano line shape in the framework of the q-exponential function proposed by Constantino Tsallis and his statistics. Besides asymmetry, the decompositions with q-BWF line shapes are stressing Gaussian and non-Gaussian behaviors of components. The data analysis of $CaO-RE_2O_3-Al_2O_3-SiO_2$ glasses is highlighting the presence of photoluminescence regular patterns in the Raman broad scans. In another database, the Raman Open Database (ROD), we can find some spectra of rare-earth oxides. Therefore, it is possible to compare the available REO spectra with those of $CaO-RE_2O_3-Al_2O_3-SiO_2$ glasses and study the broadening of the Raman bands.

Keywords: Raman Spectroscopy, Photoluminescence, Broad Scan Spectrum, Broadening of Lines, Spectrum Decomposition, q-Gaussian Tsallis Lines, Breit-Wigner-Fano Line Shape, q-BWF Line Shape

Introduction

Recently, in 2023, we proposed the q-BWF function as a generalization of the Breit-Wigner-Fano (BWF) line shape, to obtain an asymmetric form of the q-Gaussian function, to be applied to the decomposition of Raman spectra. The BWF line shape is a modified Lorentzian function, which is used to consider the asymmetry due to Fano resonance (Bianconi, 2003, Miroshnichenko et al, 2010). In fact, Ferrari and Robertson, 2000, contemplated the BWF function as suitable to describe asymmetries in the case of the Raman spectroscopy of carbonaceous material. The generalization we proposed in 2023 is using, in the BWF line, a q-Gaussian line shape instead of a Lorentzian profile. A q-Gaussian is a function based on the Tsallis q-form of the exponential function (Tsallis, 1988); this generalized exponential is characterized by a q-parameter and when q is equal to 2, we have the Lorentzian function. If q is close to 1, we have a Gaussian function (this is the reason why the Tsallis function is also known as "q-Gaussian"). For values of q between 1 and 2, we have a bell-shaped function with power-law wings ranging from Gaussian to Lorentzian tails. As shown on many occasions, the q-Gaussian is suitable for fitting Raman spectra (Sparavigna 2023,2024).

Let us write the BWF as follow:

$$BWF = C\left[1 - \xi\gamma^{1/2}(x - x_o)\right]^2 \left[1 + \gamma(x - x_o)\right]^{-1}$$

where x_o is the center of the line. When parameter ξ is zero, *BWF* becomes a Lorentzian function. Therefore, it is easy to turn BWF into a q-BWF function:

$$q\text{-}BWF = C\left[1 - \xi\gamma^{1/2}(q-1)^{1/2}(x - x_o)\right]^2 \left[1 + (q-1)\gamma(x - x_o)^2\right]^{1/(1-q)}$$

Please consider that in literature about Fano resonance the parameter ξ is often given as 1/q (and with an opposite sign). Here the q-parameter is related to the Tsallis statistics.

The *q-BWF* functions have been applied to the study of the Raman spectra of molybdenite, that is, the molybdenum disulfide, MoS_2. Due to good result we obtained in that case, we start trying to apply q-BWFs to other cases, using them to highlight asymmetries and a behavior of the line shape different from the usual Lorentzian or Gaussian profile. For Molybdenite, we used the Raman spectra from RRUFF database (Lafuente et al., 2015). Here we investigate glasses. The spectra that we find in RRUFF are those of $CaO-Al_2O_3-SiO_2$ systems with Rare Earth Element (REE) oxides.

RRUFF REO Glasses

Cairns et al., 2007, prepared rare earth element (REE) standards, according to the method

described in rruff.info . "The finished glass contains SiO_2, Rare Earth (RE) oxide [REO] (generally RE_2O_3), CaO and Al_2O_3. The gels were made in a similar manner to that described in Biggar and O'Hara (1969). The gel starting materials were prepared by mixing the required weights of standard solutions of aluminium, calcium and rare earth nitrates to produce a final weight of either 5g or 10g. Ethanol was then added to the nitrate mixture. This was to ensure the miscibility of tetraethyl orthosilicate …, used for the silica component, which was added next. Concentrated ammonia … was then added to form a gelatinous precipitate of hydroxides. The mixture was then covered and left for at least 16 hours to ensure the complete hydrolysis of the TEOS. The gels were then slowly dried," … etc. (Cairns et al., 2007).

The rare earth elements (REE) set consists of 17 chemical elements, that is the fifteen lanthanides, plus scandium and yttrium. "Compounds known as rare earth oxides (REO) are readily formed from rare earth elements as they are typically very reactive with oxygen in the ambient atmosphere" (Mo-Sci, 2023). Industries regarding "catalysts, glassmaking, lighting, and metallurgy, have been using rare earth elements for a long time. Such industries, when combined, account for 59% of the total worldwide consumption" (Mo-Sci, 2023). Newer application areas are concerning battery alloys and ceramics. For glass production, the addition of REOs changes the properties of glasses. "The ability to change the fluorescent properties of the glass is one of the most important uses of REO in glass" (Mo-Sci, 2023).

A recent editorial by Zhang & Zhang, 2022, stresses that the "trivalent rare earth ions (Ln3+) have the unique electronic configurations $[Xe]4f^n$ (n = 0–14) and numerous energy levels, which endow rare earth luminescent materials with many fascinating optical properties over a broad spectral region ranging from the ultraviolet (UV) to the near infrared (NIR); these include tunable atomic-like excitation/emission spectra, large Stokes/anti-Stokes shifts, long luminescent lifetimes, and excellent photostability" (Zhang & Zhang, 2022, and references therein). "As we entered the 21st century, nano research on rare earth luminescent materials began to unfold rapidly", and Zhang and Zhang illustrate the several cases. A review of the most traditional applications and of developments in unconventional fields has been given by Locardi and Guadagnino, 1992. About the REE doped glasses for displays and light generation, a discussion is available in Caldiño et al., 2014. However, it is necessary to note that "rare earth elements (REEs), critical to modern industry, are difficult to separate and purify, given their similar physicochemical properties originating from the lanthanide contraction" (Wang et al., 2024). Wang and coworkers propose a study of the transport of lanthanide ions (Ln3+) "in artificially confined angstrom-scale two-dimensional channels using MoS_2-based building blocks in an aqueous environment". The researchers claim that their work on artificial confinement can be useful for a "greener REEs separation".

CaO-Al_2O_3-SiO_2 (CAS) systems

These systems produce the calcium aluminosilicate (CAS) glasses. "The glass-forming region for calcium aluminosilicate glasses has been determined" by Shelby, 1985. However, "the formation mechanism and crystallization process of glass phases are still unclear" (Xin & Guo, 2022). In their work, "the glass phase and the crystallized samples of the $CaO-SiO_2-Al_2O_3$ system were characterized using X-ray diffraction, optical microscopy, scanning electron microscopy, energy-dispersive spectroscopy and Raman spectroscopy. … The results showed that the chemical composition significantly influences the crystallization of the $CaO-SiO_2-Al_2O_3$ glass" (Xin & Guo, 2022). Decreasing the basicity and the mass ratio of CaO and SiO_2 is favoring the crystallization of the glass phase; increasing the content of Al_2O_3 is inhibiting the crystallization of the glass phase (Xin & Guo, 2022). Actually, "among the materials available, $CaO-Al_2O_3-SiO_2$ (CAS) is a predominant ternary glass-ceramic system" with great potential applications (Fang et al., 2021, and references therein).

Raman spectroscopy and photoluminescence

"Raman scattering is a weak phenomenon and that is sometimes the reason for being unable to acquire a Raman spectrum, particularly at a low concentration or with a limited amount of sample. However, the most frequent reason for not being able to acquire a Raman spectrum is because a strong fluorescent background and the detector noise generated by it overwhelms the Raman signal. Therefore, it should be self-evident that a Raman spectrometer is ideal for performing laser-excited photoluminescence" (Tuschel, 2016). Absorbing a photon, an electron is promoted to an excited level of energy. It can decay emitting a photon. This "emission process is called photoluminescence", since "the excited state was reached through the absorption of a photon … Photoluminescence occurs in many bulk materials that are direct band gap semiconductors and also because of impurities that absorb and emit light in an otherwise transparent medium" (Tuschel, 2016).

As told also by Yu et al., 2014, "fluorescence or laser-excited luminescence has always been considered troublesome in Raman spectroscopy,

since they easily mask the much weaker Raman signals and degrade the quality of the spectra. People have developed several strategies to eliminate the bad influence of fluorescence, … but it is still difficult to obtain pure Raman spectra without fluorescence interference in many cases" (see references in Yu et al.). For *lanthanide materials*, the situation becomes even worse because most of the lanthanide ions are luminescent and abundant luminescence bands are commonly seen in Raman spectra of them, which makes the interpretation of such spectra sometimes rather difficult. However, *see this problem from a different view*, fluorescence signals generated in Raman spectroscopy sometimes can also be helpful, since they may provide useful additional information of the material" (Yu et al., 2014). The previous research made by Yu and coworkers "indicates that Raman spectroscopy is ultrasensitive to lanthanide luminescence and thus can be utilized for detecting trace lanthanide impurities" (Yu et al., 2014). In the article by Yu and coworkers, we find the Raman spectra of rare earth sesquioxides RE_2O_3 (RE=Eu, Gd, Dy, Ho, Er, Tm, Yb, Lu, Sc and Y).

In general, as observed by Sadagov et al., 2020, "increasing employment of Raman spectroscopy for the qualitative and quantitative analyses of substances and materials requires to record accurate and device-independent Raman spectra. … To ensure the independence of the Raman spectra on the hardware, it is necessary to solve the following two problems", which are regarding the "calibration of the Raman spectrometer with respect to the wavenumber scale" and the calibration "with respect to the shape of the spectra, i.e., with respect to the relative intensities of the Raman peaks" (Sadagov et al., 2020). For what is regarding the special glass compositions, "the following requirements are imposed" by NIST: "(a) sufficiently strong fluorescence under the influence of laser radiation that excites Raman scattering, which is capable of ensuring Stokes shifts in the wavenumber range from 200 to 4000 cm^{-1}; (b) photostability; and (c) low absorption at the wavelength of exciting radiation, which is required to prevent heating caused by laser radiation" (Sadagov et al., 2020). Sadagov and coworkers studied the "fluorescence calibration standards based on phosphate matrix glass activated with ions of rare-earth metals".

Broad scans
As previously told, here we will consider the RRUFF Raman data of REO glass standards, which are courtesy of Elizabeth Cairns, University of Edinburgh. We consider the broad scans from 0 to 6000 cm^{-1}.
"The area from 0 to about 1600 cm^{-1} is the so-called Raman "fingerprint zone". The spectral pattern of this area reflects a fingerprint enabling the identification of a material, just as a fingerprint enables the identification of a person. This is also the area in which most Raman signals of inorganic solids occur". Usually, spectra are recorded "only across fingerprint zone, … Fingerprint spectra are also typically background corrected. This means any slope generated by luminescence has been subtracted from the spectrum. Background correction prepares the data for the computer to find the peak locations and match them against a library containing spectra of known materials" (GemmoRaman, 2012). "The extended area from 0 to about 3000-6000 cm^{-1} (depending on spectrometer) is called a *broad scan area*. Broad scan contains both Raman fingerprint zone and an extended range for photoluminescence studies. The line between the zones is not very distinct. Photoluminescence reactions do occur at both areas and sometimes mix with or overwhelm any Raman signals. … For gemology it is advisable to pay attention to luminescence as much as Raman signals, because it often contains important information about chromophores (such Cr) and rare earth elements (REE)" (GemmoRaman, 2012).

"The key skill in spectra interpretation is to learn how to see "overlapping peaks" by looking for deviations in peak formation. These deviations show up usually so that a peak does not follow nice Gaussian distribution" (GemmoRaman, 2012).

RRUFF Glass-(Ce) R110075 - Cerium, atomic number 58, is an element classified as a lanthanide, pubchem.ncbi.nlm.nih.gov/element/Cerium. The glass contains the Cerium oxide. RRUFF provides information about the measured chemistry of glass: CaO 16.44%, Ce_2O_3 19.71%, Al_2O_3 10.13%, SiO_2 53.72%, $Ca_{11}Ce_5Al_8Si_{35}O_{100}$, and about Raman measurement: spectrum overwhelmed by fluorescence, instrument setting Thermo Almega XR 532 nm @ 100% of 150 mW.

Here in the following, the Raman broad scan is given with a baseline adjustment. The spectrum is decomposed by means of Fityk software, where q-BWF functions are defined (see Appendix for details).
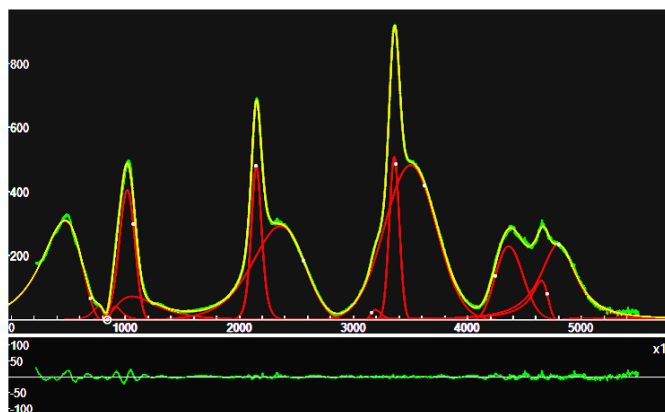
Fig.1: Raman broad scan RRUFF Glass-(Ce) R110075 (green) decomposed in q-BWF functions (red curves). The sum of these components is given in yellow. In fact, green data and yellow line are practically undistinguishable. In the lower part of the image, the misfit is given, that is, the difference between green data and yellow line.
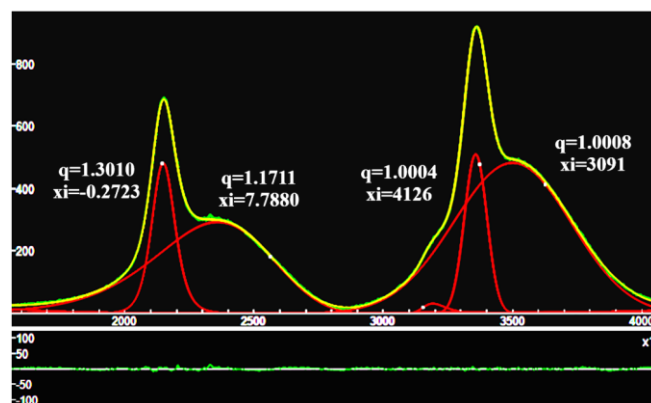

Fig.2: Four q-BWF components of the spectrum and the values of their q and xi parameters. Note that when the parameter q is close to 1, to have asymmetry, we need to strongly increase the parameter xi. Note also the white dots, they are representing the "center" of the components. In the case of q-BWF, such as for BWF, the "center" does not coincide with the maximum of the component.

From the Figure 2, we can see that the band between 1700 and 2800 cm^{-1} is made of functions which are not Gaussians, besides being asymmetric. Let us compare the decompositions of this band in the case that, for the decomposition of the total spectrum, q-BWF functions or Gaussians are used. The comparison is proposed in the Fig.3.
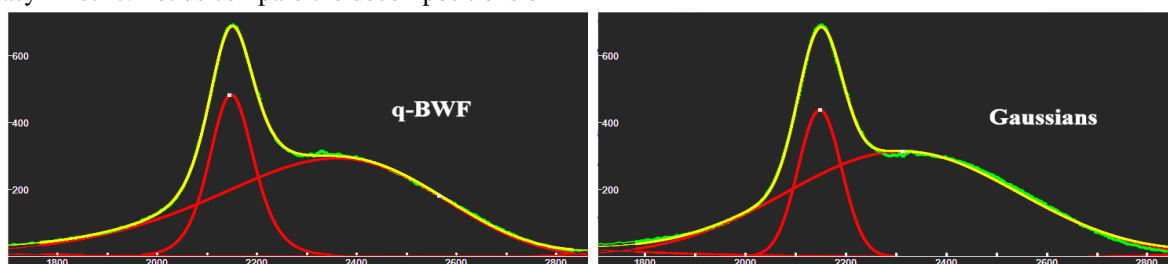

Fig.3: Comparing decomposition with q-BWF functions and Gaussians.

RRUFF Glass-(Gd) R110080 - Gadolinium, atomic number 64, lanthanide, pubchem.ncbi.nlm.nih.gov/element/64. Measured chemistry of glass: CaO 19.29%, Gd$_2$O$_3$ 20.85%, Al$_2$O$_3$ 11.71%, SiO$_2$ 48.16%, Ca$_{14}$Gd$_5$Al$_9$Si$_{33}$O$_{100}$. Raman measurement: spectrum overwhelmed by fluorescence, instrument setting Thermo Almega XR 532 nm @ 100% of 150 mW.

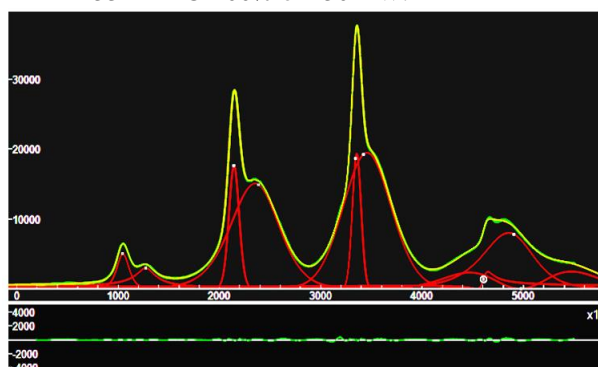Fig.4: Raman broad scan RRUFF Glass-(Gd) R110080 decomposed in q-BWF functions.
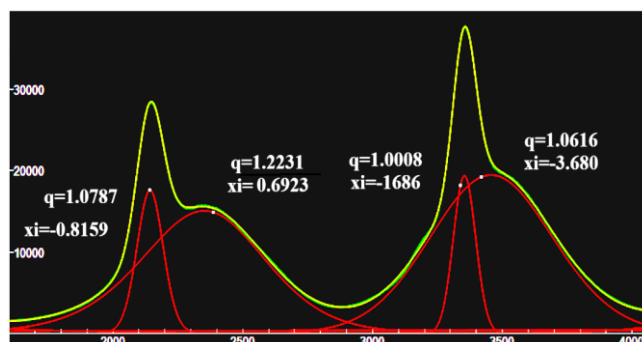

Fig.5: Four q-BWF components of the spectrum and the values of their q and xi parameters. Note that when the parameter q is close to 1, to have asymmetry, we need to strongly increase the parameter xi.

We can compare the position of the peaks in RRUFF Glass-(Ce) R110075 and RRUFF Glass-(Gd) R110080.
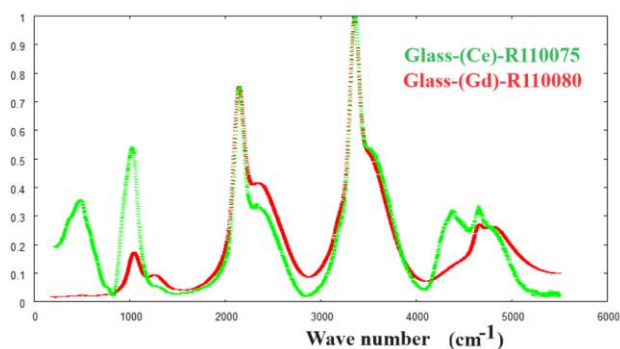
As in the case of the Figure 2, let us consider the parameters of the two central bands. The result is given in the following Figure 5.

Fig.6: Comparison of the Raman spectra. Intensities in arbitrary units.

Glass-(Sm) R110078 - Samarium, atomic number 62, lanthanide, pubchem.ncbi.nlm.nih.gov/element/62. Measured chemistry of glass: CaO 19.44%, Sm_2O_3 20.20%, Al_2O_3 11.81%, SiO_2 48.55%, $Ca_{14}Sm_5Al_9Si_{33}O_{100}$. Raman measurement: spectrum overwhelmed by fluorescence, instrument setting Thermo Almega XR 532 nm @ 100% of 150 mW.
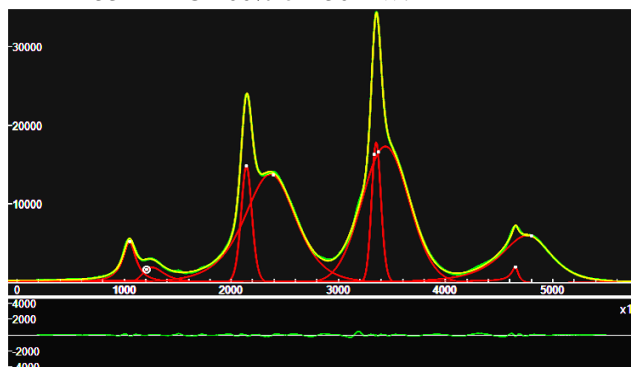

Fig.7: Raman broad scan RRUFF Glass-(Sm) R110078 decomposed in q-BWF functions.

Let us compare the positions of the peaks in RRUFF Glass-(Sm) R110078 and RRUFF Glass-(Gd) R110080.
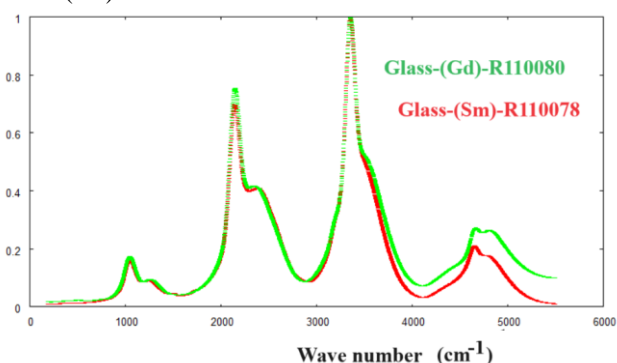

Fig.8: Comparison of the Raman scans. Intensities in arbitrary units.

RRUFF Glass-(Ho) R110083 - Holmium, atomic number 67, lanthanide, pubchem.ncbi.nlm.nih.gov/element/67 . Measured chemistry of glass: CaO 19.38% Ho_2O_3 21.77%, Al_2O_3 11.72%, SiO_2 47.13%, $Ca_{14}Ho_5Al_9Si_{32}O_{100}$. Raman measurement: spectrum overwhelmed by fluorescence, instrument setting Thermo Almega
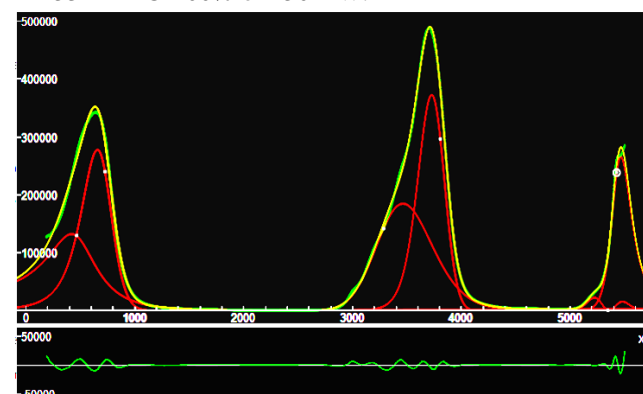
XR 532 nm @ 100% of 150 mW.

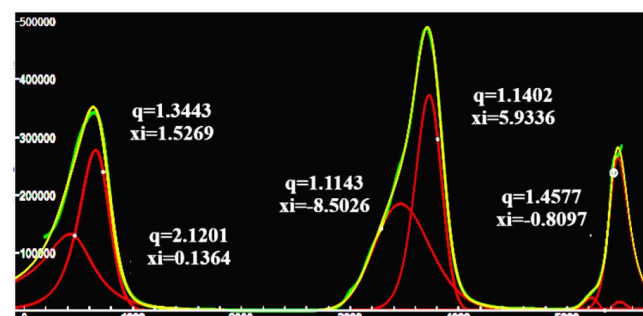Fig.9: Raman broad scan RRUFF Glass-(Ho) R110083 decomposed in q-BWF functions.

Fig.10: q-BWF components of the spectrum in the Fig.7 and the values of their q and xi parameters.

RRUFF Glass-(Tm) R110085 - Thulium, atomic number 69, lanthanide, pubchem.ncbi.nlm.nih.gov/element/69 . Measured chemistry of glass: CaO 22.78%, Tm_2O_3 26.12%, Al_2O_3 13.80%, SiO_2 37.30%, $Ca_{18}Tm_6Al_{12}Si_{28}O_{100}$. Raman measurement: spectrum overwhelmed by fluorescence, instrument setting Thermo Almega XR 532 nm @ 100% of 150 mW.
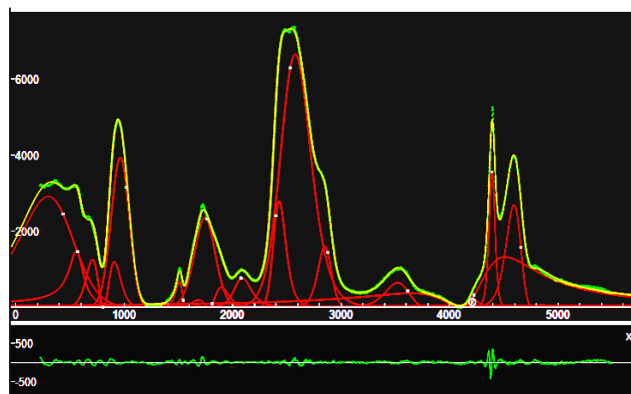

Fig.11: Raman broad scan RRUFF Glass-(Tm) R110085 decomposed in q-BWF functions.

RRUFF Glass-(Lu) R110087 - Lutetium, atomic number 71, lanthanide, pubchem.ncbi.nlm.nih.gov/element/71 . Measured chemistry of glass: CaO 18.91%, Lu_2O_3 22.31%, Al_2O_3 11.49%, SiO_2 47.29%, $Ca_{14}Lu_5Al_9Si_{33}O_{100}$. Raman measurement: spectrum overwhelmed by fluorescence, instrument setting Thermo Almega
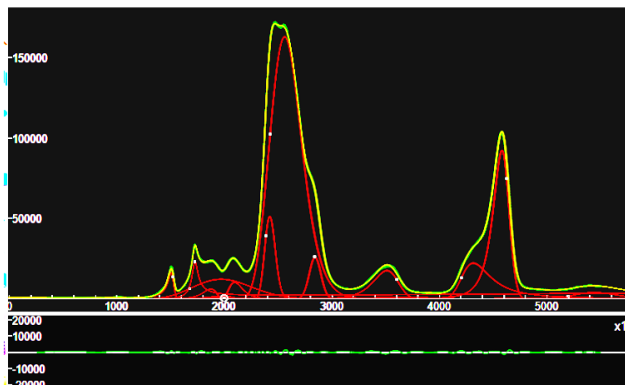
XR 532 nm @ 65% of 150 mW.

Fig.12: Raman broad scan RRUFF Glass-(Lu) R110087 decomposed in q-BWF functions.

Once more, let us compare the positions of the peaks in RRUFF Glass-(Tm) R110085 and RRUFF Glass-(Lu) R110087.
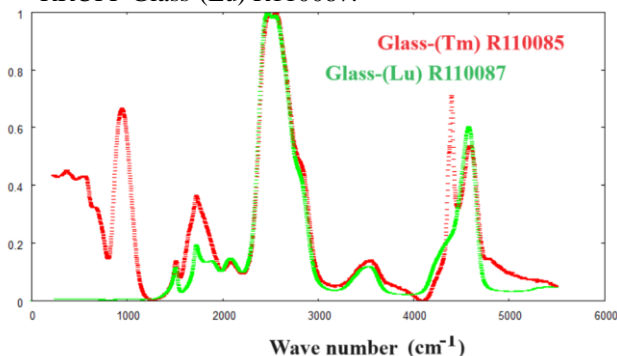

Fig.13: Comparison of the Raman scans. Intensities in arbitrary units.

RRUFF Glass-(Eu) R110079 - Europium, atomic number 63, lanthanide, pubchem.ncbi.nlm.nih.gov/element/63 . Measured chemistry of glass: CaO 21.74%, Eu_2O_3 23.09%, Al_2O_3 13.24%, SiO_2 41.93%, $Ca_{16}Eu_6Al_{11}Si_{29}O_{100}$. Raman measurement: spectrum overwhelmed by fluorescence, instrument setting Thermo Almega XR 532 nm @ 1% of 150 mW.
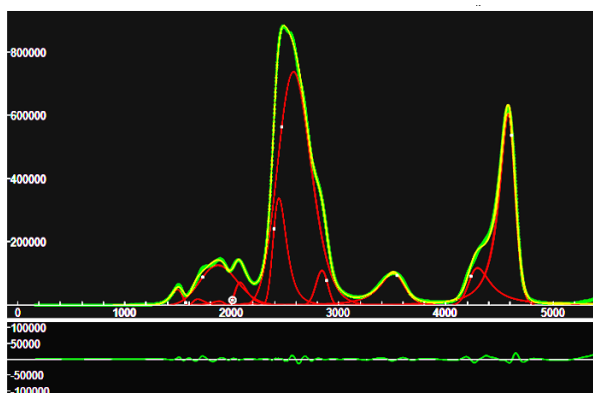

Fig.14: Raman broad scan RRUFF Glass-(Eu) R110079 decomposed in q-BWF functions.

Comparison of the positions of peaks in RRUFF Glass-(Eu) R110079 and RRUFF Glass-(Lu)

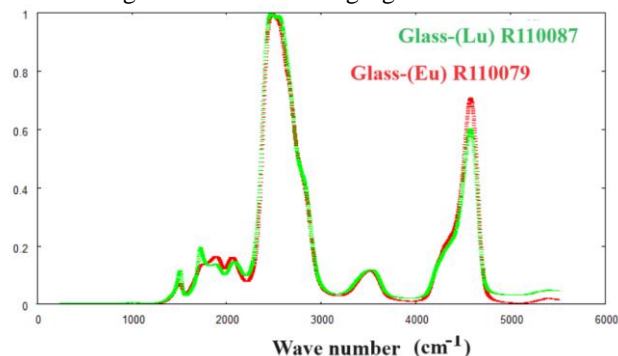R110087 is given in the following figure.

Fig.15: Comparison of the Raman scans. Intensities in arbitrary units.
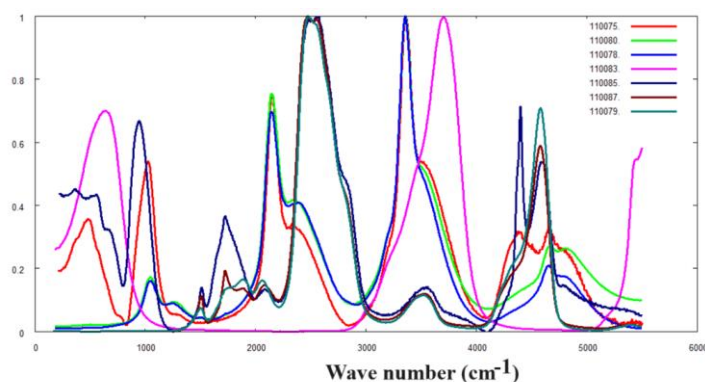
All the spectra seen before

Fig.16: Spectra from RRUFF of glasses with Ce, Gd, Sm, Ho, Eu, Tm and Lu oxides.

In the Figure 16, we show the spectra seen before, with relative intensities (largest value equal to 1). We can note the presence of three regular luminescence patterns in the Raman broad scans. We have the set of patterns for R110075 (Ce), R110080 (Gd), R110078 (Sm). The peaks as in the Figs. 2 and 5 remember the patterns of ice/water systems (Sparavigna, 2024). Then we have the single R110083 (Ho). The third set of patterns is that of R110079 (Eu), R110085 (Tm), R110087 (Lu). Note please that for R110075, R110085, R110087 we have used the RRUFF data adjusted with a baseline. The use of a baseline could be questionable, but here is adopted to evidence the patterns in the spectra.
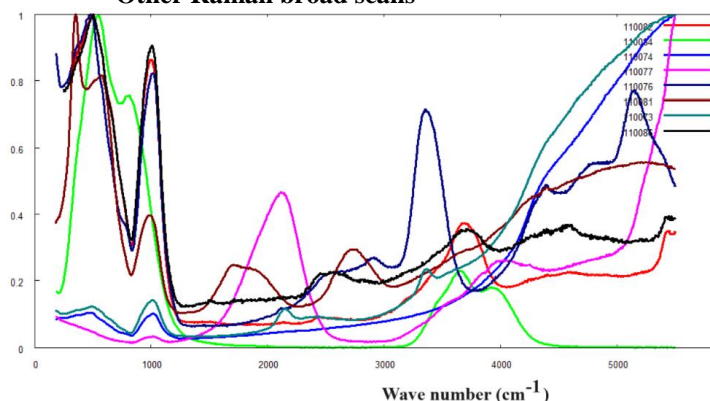
Other Raman broad scans

Fig.17: Spectra from RRUFF of glasses with Dy, Er, La, Nd, Pr, Tb, Y and Yt oxides.

Other Raman broad scans courtesy Elisabeth Cairns are given in RRUFF database. Here we propose them as in the Fig.17. The figure is showing R110082 (Dy), R110084 (Er), R110074 (La), R110077 (Nd), R110076 (Pr), R110081 (Tb), R110073 (Y), R110086 (Yt). No baseline is used.
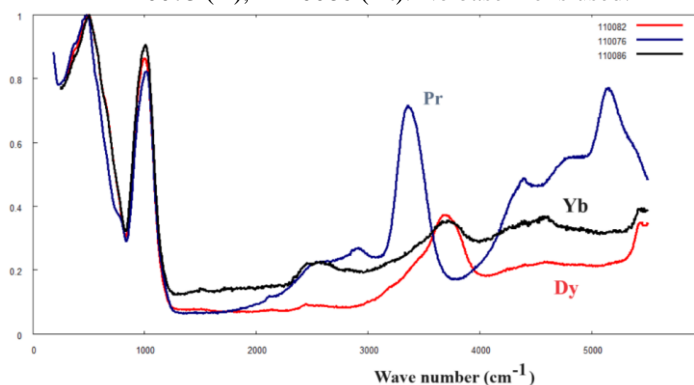

Fig.18: Spectra from RRUFF of glasses with Dy, Pr and Yb.

In the Figure 18, we propose the cases of Glass-(Dy), Glass-(Pr) and Glass-(Yb) to compare their Raman broad scans. Interesting the common peak at about 1000 cm^{-1}.

Electronic and Optical Properties of RE Ions

Before discussing specific cases of spectra, let us consider Miniscalco, 2001, and his work about the optical and electronic properties of rare earth ions in glasses. "Rare earth ions have a long history in optical and magnetic applications. Among these, luminescent devices using single crystals, powders, and glasses have been particularly important". The use of rare earths is due to their important characteristics: "they emit and absorb over narrow wavelength ranges, the wavelengths of the emission and absorption transitions are relatively insensitive to host material, the intensities of these transitions are weak, the lifetimes of metastable states are long, and the quantum efficiencies tend to be high, except in aqueous solutions. These properties all result from the nature of the states involved in these processes and lead to excellent performance of rare earth ions in many optical applications. Devices that provide gain, such as lasers and amplifiers, must have low scattering losses, and one is restricted to using single-crystal or glass hosts. Whereas in many applications crystalline materials are preferred …, the versatility of glasses and the broader emission and absorption spectra they provide have led to the use of rare earth doped glasses in many applications. Nowhere is this more true than in the area of optical fiber devices." (Miniscalco, 2001).

Miniscalco remembers that "lanthanides are characterized by the filling of the 4f shell and begin with cerium (Ce), which has an atomic number Z of 58, and end with lutetium (Lu, Z 71)". An observation: "The name *rare earth* is, in fact, a misnomer, for lanthanides other than Pm are not actually rare, and the elements with even atomic numbers are particularly abundant". Miniscalco observes that, "from the perspective of optical and electronic properties, the most important feature of rare earths is the lanthanide contraction", which is discussed by the researcher. "While neutral lanthanum (La) has the xenon structure plus 5d6s^2, the electrons that are added for the neutral elements that follow are found in the 4f shell and only Ce, gadolinium (Gd), and Lu have a 5d electron. … In condensed matter the trivalent (3) level of ionization is the most stable for lanthanide ions, and most optical devices use trivalent ions. … Ionization preferentially removes the 6s and 5d electrons, and the electronic configuration for these ions (henceforth, referred to as rare earth ions) is that of the xenon structure plus a certain number (1–14) of 4f electrons" (Miniscalco, 2001).

The line-broadening mechanisms are also discussed. "For rare earth doped crystals, the absorption and emission transitions between Stark components of different J multiplets usually can be observed at room temperature as discrete lines. In contrast, individual Stark transitions for glass hosts seldom can be resolved except at temperatures close to absolute zero. This difference is illustrated in Figure 6 (Miniscalco, 2001), which compares the 1060-nm emission of Nd^{3+}:YAG with that of an Nd^{3+}-doped silicate glass at room temperature. … [Let us note that] crystalline hosts provide high cross sections at nearly discrete wavelengths while glass hosts have lower cross sections over a broad, continuous range of wavelengths. … Both homogeneous and inhomogeneous processes are responsible for broadening the sharp line structure of the crystal into that seen for the glass. The relative contribution of each mechanism has important device implications, and there has been

considerable interest in understanding these mechanisms" (Miniscalco, 2001). Miniscalco continues with the discussion of the homogeneous broadening. "The other broadening mechanism is called inhomogeneous because it results from spectroscopic differences between individual ions. This situation arises because each dopant ion occupies a unique site in a glass and experiences different crystal field parameters". Disorder leads to a distribution of energies and, "in a measurement that samples all ions, inhomogeneously broadens the emission and absorption spectra" (Miniscalco, 2001).

Europium oxide
Let us consider more specifically the Raman spectrum of Eu_2O_3. To understand R110079 (Eu), let us consider Zhao et al., 2004. The researchers studied Eu_2O_3 doped $5ZnO-20Nb_2O_5-75TeO_2$ glasses. In this case, "Raman spectra show that Eu_2O_3 dopant induces the changes in the local structure of glasses. The higher the dopant concentration, the larger the nonlinear refractive n_2 and the faster the temporal response. The Figure 3 in Zhao et al. gives the Raman spectra for different concentrations of Eu_2O_3 dopants. There are characteristic Raman peaks of 470 and 740 cm^{-1}. For the investigated material, "the former may be attributed to the stretching vibration of non-bridge oxygen and tellurium in the glassy framework, … . The latter may be attributed to the symmetric stretching vibration of O-Te-O chains" (Zhao et al. mentioning Sidebottom et al., 1997). The corresponding Raman peak intensity is decreasing with increasing Eu_2O_3 dopant concentration, as shown by Figure 3 in Zhao et al., 2004. "Furthermore, the 532 nm excited laser gives rise to the transitions of $^5D_0 \rightarrow {}^7F_{0,1,2,3,4}$ (Zhao et al. mentioning Kumar et al., 2002), resulting in Raman scattering at 2504.3 cm^{-1}, and their intensity increase with the increasing Eu_2O_3 concentration". In our Figure 14, the large peak is at about 2480 cm^{-1}. In the Figure 3 by Zhao et al., we can see also a peak at 4532.5 cm^{-1}. In our Figure 16, the peak is at about 4582 cm^{-1}.

In Yu et al., 2014, it is told that for Eu_2O_3, "since Eu^{3+} can effectively be excited by 532 nm laser, the spectrum collected with 532 nm excitation presents strong intrinsic luminescence of Eu^{3+}, which totally masks the low-wavenumber Raman bands. Based on the well investigated energy levels of Eu^{3+}, the luminescence band at 2500 cm^{-1} can be assigned to $^5D_0 \rightarrow {}^7F_2$ transition of Eu^{3+} (Yu et al. mentioning Wakefield et al., 2001)". Moreover, "similar luminescence bands were observed in Raman spectra of Gd_2O_3 and Sc_2O_3 with 532 nm excitation, which indicates that they both contain Eu^{3+} impurity" (Yu et al., 2014).

Eu_2O_3 in ROD
Another database is the Raman Open Database, ROD (El Mendili et al., 2019, El Mendili, 2017). There, we can find the Raman spectrum of commercial Eu_2O_3 (chemical compound source: commercial LABOSI 99.9%). Information, given by solsa.crystallography.net/rod/3500047.html, tells us that the Raman spectrum was recorded under the following conditions: excitation wavelength 532 nm, measurement resolution 3 cm^{-1}, unoriented sample, power on the sample 1 mW, company of the measurement device Thermo Scientific, Model DXR.

Let us consider the spectrum from 2200 to 3200 cm^{-1}. The spectrum and a decomposition obtained using the q-Gaussian functions are given in the following Fig. 19. The q-Gaussians are symmetric functions. Centers of the main q-Gaussians are 2430.5, 2469.0, 2510.0, 2537,0, 2566.0, 2742.5 and 2861.0 cm^{-1}.
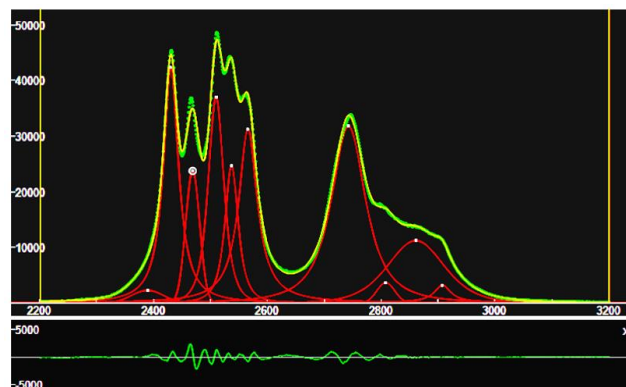

Fig.19: A part of the Raman broad scan ROD Eu_2O_3 3500047 (green) decomposed in q-Gaussian functions (red curves). The sum of these components is given in yellow. In the lower part of the image, the misfit is given, that is, the difference between green data and yellow line. To obtain the decomposition, a baseline has been applied.

As told by Kumar et al., 2002, "the rare earth absorption and fluorescence spectra are quite sensitive to the local environment of the ion". In Malba et al., 2015, too we find that the "rare earths luminescence is sensitive to the local environment and can experience a line broadening passing from an ordered state to a more disordered or dynamic system" (Malba et al. mentioning Meltzer, 2005). Therefore, if we pass from the crystalline phase to an amorphous state, the bands related to the $7^5D_0 \rightarrow {}^7F_{0,1,2,3,4}$ turn out to be broadened. To stress the broadening of the lines, let us consider again the glass $CaO-Eu_2O_3-Al_2O_3-SiO_2$ from RRUFF 110079, in the same range from 2200 to 3200 cm^{-1}, as in the Figure 20 on the right. On the left, the Raman band of Eu_2O_3.
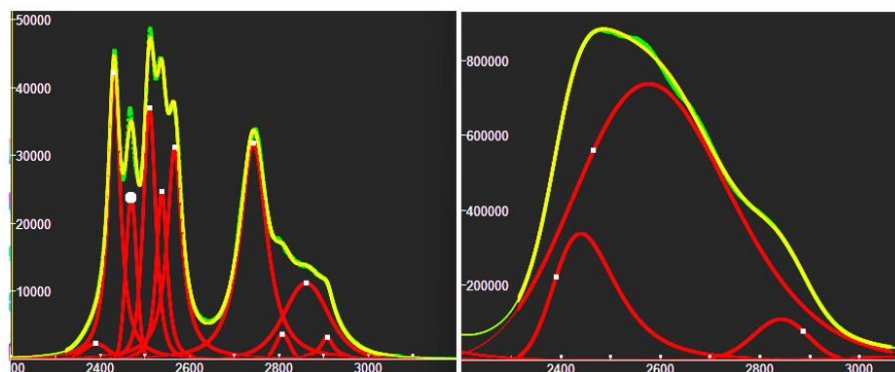
Fig.20: Broadening of the lines. On the left, the commercial Eu_2O_3 oxide, on the right the $CaO-Eu_2O_3-Al_2O_3-SiO_2$ glass.
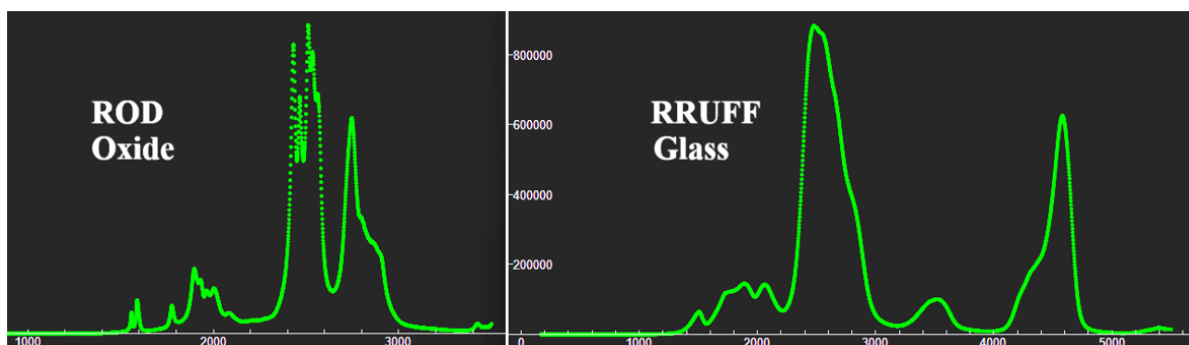
Fig.21: On the left, the ROD spectrum of commercial Eu_2O_3 oxide, on the right the RRUFF spectrum of $CaO-Eu_2O_3-Al_2O_3-SiO_2$ glass.

Holmium Oxide in ROD

The ROD spectrum is available at solsa.crystallography.net/rod/3500009.rod (El Mendili, 2017). Regarding another research on this oxide, Pandey et al. (2014) studied Raman scattering of Ho_2O_3 dependent on pressure and temperature.
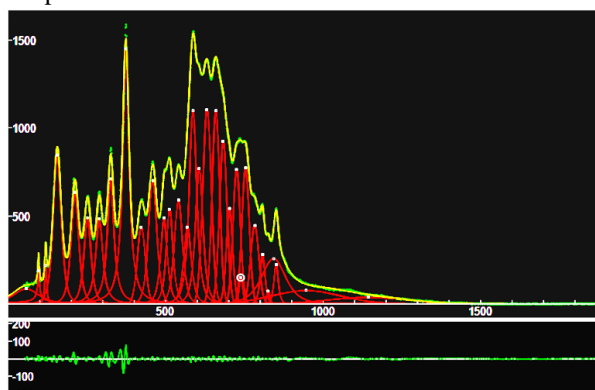
Fig.22: A part of the Raman broad scan ROD Ho_2O_3 3500009 (green) decomposed in q-Gaussian functions (red curves). The sum of these components is given in yellow. In the lower part of the image, the misfit is given, that is, the difference between green data and yellow line. No baseline has been applied.

Let us compare the spectra of oxide and glass, as in the Fig.23, to observe the result of the broadening of lines.

Fig.23: Broadening of the lines. On the left, the commercial Eu_2O_3 oxide, on the right the $CaO\text{-}Eu_2O_3\text{-}Al_2O_3\text{-}SiO_2$ glass.

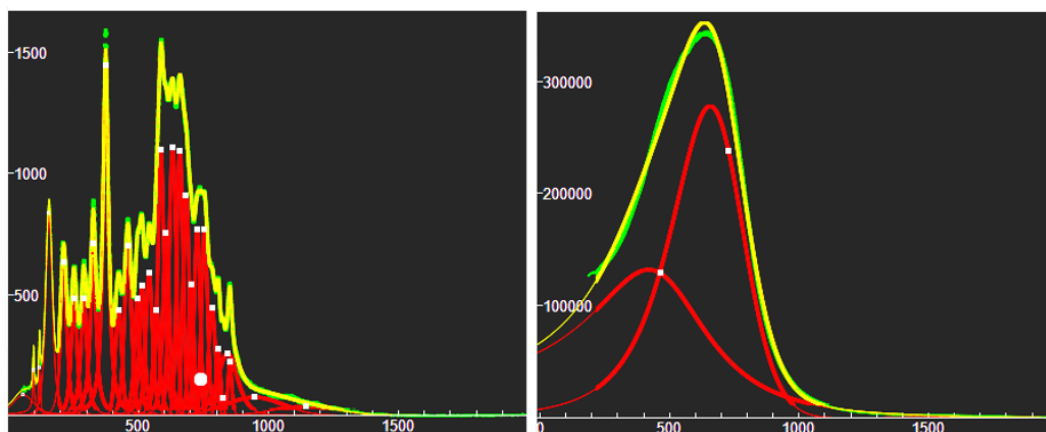**Erbium, Neodymium, Samarium**

In ROD we can find also the oxides of Er, Nd, Sm, Y, Ce and Gd. So let us consider these cases too. Again, the aim is that of evidencing the role of environment on the Raman spectral bands. Erbium oxide spectrum (El Mendili, 2017), 3500007.rod , is given in the Fig.24a, Neodymium oxide spectrum (El Mendili, 2017), 3500066.rod, Fig.24b, and Samarium oxide spectrum (El Mendili, 2017), 3500097.rod, in the Figure 24c.
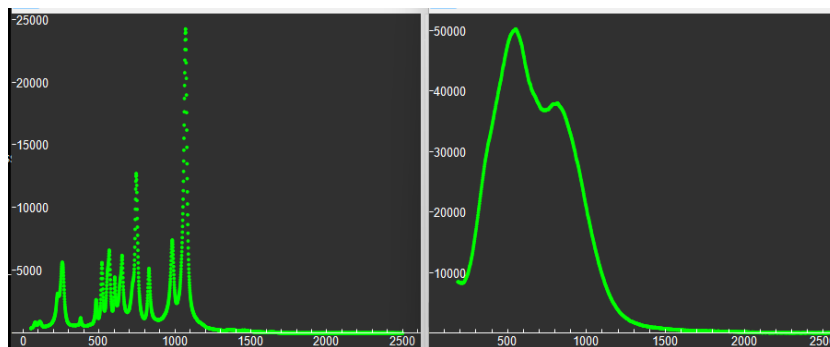

Fig.24a: On the left, the commercial Er_2O_3 oxide, on the right the $CaO\text{-}Er_2O_3\text{-}Al_2O_3\text{-}SiO_2$ glass.
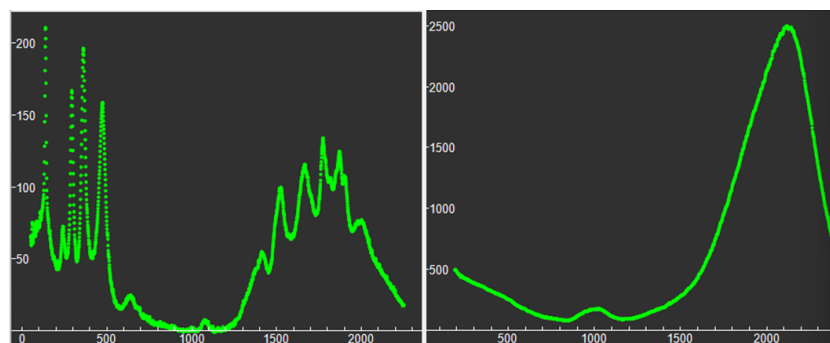

Fig.24b: On the left, the commercial Nd_2O_3 oxide, on the right the $CaO\text{-}Nd_2O_3\text{-}Al_2O_3\text{-}SiO_2$ glass.

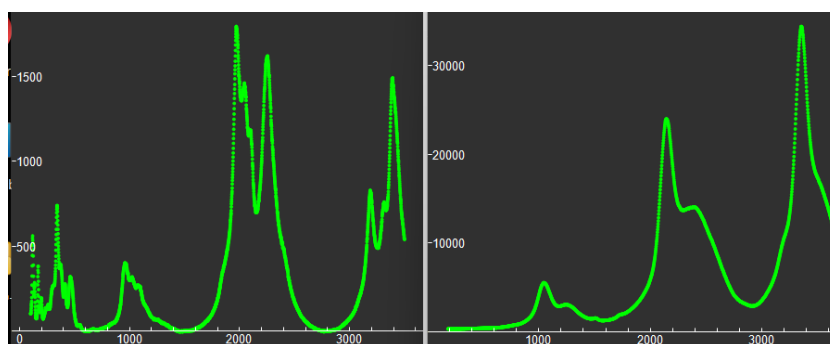
Fig.24c: On the left, the commercial Sm_2O_3 oxide, on the right the $CaO\text{-}Sm_2O_3\text{-}Al_2O_3\text{-}SiO_2$ glass.

The three cases shown in the Figures 24a, b, and c, seem being interesting, as those given in Figs. 20 and 23. However, for Yttrium, Cerium and Gadolinium, the comparison is unsuccessful.

For what is regarding the crystal phases, the rare-earth oxides have been studied by Roth and Schneider, 1960, to find the polymorphic relationships of phases. "The oxides of the trivalent rare earth ions crystallize in three different types: A, B, and C. Each oxide has only one truly stable polymorph: La_2O_3, Ce_2O_3, Pr_2O_3, and Nd_2O_3 belong to the A type; Sm_2O_3, Eu_2O_3, and Gd_2O_3 to the B type; Tb_2O_3, Dy_2O_3, Ho_2O_3, Er_2O_3, Tm_2O_3, Yb_2O_3, and Lu_2O_3 to the C type. In addition Nd_2O_3, Sm_2O_3, Eu_2O_3, and Gd_2O_3 have low-temperature, apparently metastable, C-type polymorphs". For the description of A, B, C types, see please the discussion in Roth and Schneider, 1960.

Role of environment
According to Geissinger and coworkers, the "molecular electronic states are extremely sensitive to changes in their environment. Therefore, by inserting probe molecules into a host material and monitoring the ensuing changes in the widths and spectral positions of the electronic absorption bands, interactions of probe and host molecules can be studied". Consequently, a method for studying "intermolecular interactions in the condensed phase is to insert into the system of interest small concentrations of a different molecular species as probes". And, as we have seen before, REEs are suitable for this purpose too. The positions and widths of the spectral lines change due to the host material excitation modes, which can be the lattice phonons in the crystal phase, which "couple to the guest electronic states. These dynamic effects are especially prominent in disordered host materials, where low-energy excitations such as two-level tunneling systems (TLS) and (pseudo) local modes provide relaxation channels, thereby leading to an increase in homogeneous absorption line widths" (Geissinger et al., 2000). The comparison, proposed in the Figs. 20, 22 and 23, seems showing that the broadening effect, produced by the local disordered environment, of the spectral lines of rare earth chromophores is creating a mechanism able of generating the band observed in CaO-Sm_2O_3-Al_2O_3-SiO_2 glasses of Eu, Er, Ho, Nd and Sm. In the case of Y, Ce and Gd, this mechanism is not observed in the available spectra.

We have encountered the "chromophores" in the Kubo theory as proposed by Tokmakoff, 2014, who was focusing on how chromophore's interactions with its environment influence its transition frequency and lineshape, that is, how interactions produce line broadening. Tokmakoff tells that there are three cases of line broadening: homogeneous, inhomogeneous, and a more general case of "spectral diffusion", with the system positioned between the homogeneous and inhomogeneous cases (see Tokmakoff for explanation). "In condensed matter, time-dependent interactions with the surroundings can lead to time-dependent frequency shifts, known as spectral diffusion. How these dynamics influence the line width and lineshape of absorption features depends on the distribution of frequencies available to your system Δ and the time scale of sampling varying environments (τ_c)" (Tokmakoff, 2014). Tokmakoff discusses the related theory, that is the Kubo theory, and the corresponding line shapes. Actually, we have shown that the Kubo line shapes can be mimicked by the q-Gaussian line shapes. Therefore, the value of the q-parameter turns out to the related to the time scale of dynamics (fast q=2, mid q=1.4 and slow q=1) (Sparavigna, Jan 2024, Mar 2024). Being possible to consider the q-parameter as featuring the broadening mechanism related to the environmental effects on chromophores, further studies on the Raman broad scans of RE oxides are necessary.

Appendix – q-Gaussian, split-q-Gaussian and q-BWF functions
The q-Gaussian functions are probability distributions proper of the Tsallis statistics (Tsallis, 1988, Hanel et al., 2009). These functions are based on a generalized form of the exponential function, characterized by a continuous real parameter q. When q is going to 1, the q-exponential becomes the usual exponential function. The value q=2, (Naudts, 2009), corresponds to the Cauchy distribution, also known as the Lorentzian distribution; the q-Gaussian function is therefore a generalization of the Lorentzian distribution too. The change of q-parameter is allowing the q-Gaussian function to pass from the Gaussian to the Lorentzian distribution.

As given by Umarov et al., 2008, the q-Gaussian function is: $f(x) = Ce_q(-\beta x^2)$, where $e_q(.)$ is the q-exponential function and C a scale constant (in the exponent, $\beta = 1/(2\sigma^2)$). The q-exponential has expression: $e_q(u) = [1 + (1 - q)u]^{1/(1-q)}$.
To have an asymmetric form of the q-Gaussian function, let us write it in the following manner (the center of the band is at x_o):
$$q\text{-}Gaussian = Cexp_q(-\beta(x - x_o)^2)$$
$$= C\,[1 + (q - 1)\beta(x - x_o)^2]^{1/(1-q)}$$

In ChemRxiv we considered the asymmetric q-Gaussians, as given by Devi (2021):

$$q\text{-Gaussian}_{\text{LEFT}} = C exp_{q_L}(-\beta_L(x - x_o)^2) = C\,[1 + (q_L - 1)\beta_L(x - x_o)^2]^{1/(1-q_L)}, \text{ when } x - x_o < 0$$

$$q\text{-Gaussian}_{\text{RIGHT}} = C exp_{q_R}(-\beta_R(x - x_o)^2) = C\,[1 + (q_R - 1)\beta_R(x - x_o)^2]^{1/(1-q_R)}, \text{ when } x - x_o > 0$$

Parameters q and β of the Left and the Right parts are different. The most proper name for this asymmetric function is split-q-Gaussian. We have also generalized the Breit-Wigner-Fano into a q-Breit-Wigner-Fano.

In Fityk, a q-Gaussian function can be defined in the following manner:

define Qgau(height, center, hwhm, q=1.5) = height*(1+(q-1)*((x-center)/hwhm)^2)^(1/(1-q))

q=1.5 the initial guessed value of the q-parameter. Parameter hwhm is the half width at half maximum of the component. When q=2, the q-Gaussian is a Lorentzian function, that we can find defined in Fityk as:

Lorentzian(height, center, hwhm) = height/(1+((x-center)/hwhm)^2)

When q is close to 1, the q-Gaussian becomes a Gaussian function. The split q-Gaussian is defined as:

Splitqgau(height, center, hwhm1=hwhm, hwhm2=hwhm, q1=1.5, q2=1.5) = x < center ? Qgau(height, center, hwhm1, q1) : Qgau(height, center, hwhm2, q2)

The split Lorentzian is: SplitLorentzian(height, center, hwhm1=hwhm, hwhm2=hwhm) = x < center ? Lorentzian(height, center, hwhm1) : Lorentzian(height, center, hwhm2)

And the q-BWF can be defined as:

Qbreit(height, center, hwhm, q=1.5, xi=0.1) = (1-xi*(q-1)*(x-center)/hwhm)^2 * height*(1+(q-1)^0.5 *((x-center)/hwhm)^2)^(1/(1-q))

And the BWF can be defined as:

Breit(height, center, hwhm, xi=0.1) = (1-xi*(x-center)/hwhm)^2 * height/(1+((x-center)/hwhm)^2)

Using +xi instead of -xi does not change the fitting results in Fityk.

References

1. Bianconi, A. (2003). Ugo Fano and shape resonances. In AIP Conference Proceedings (Vol. 652, No. 1, pp. 13-18). American Institute of Physics.
2. Biggar, G. M., & O'hara, M. J. (1969). A comparison of gel and glass starting materials for phase equilibrium studies. Mineralogical Magazine, 37(286), 198-205.
3. Cairns, E., Choi, P. C., Fearnhead, K., Hadden, P., Hill, P., Malik, S., Saunders, M., Steele, D. & Tomlinson, E. (2007). Rare earth element (REE) standards. School of GeoSciences, The University of Edinburgh (http://www.geos.ed.ac.uk/facilities/EMMAC/electron/REESta ndards/) 1-20. Available https://rruff.info/uploads/REE%20Standards1.pdf
4. Caldiño, U., Bettinelli, M., Ferrari, M., Pasquini, E., Pelli, S., Speghini, A., & Righini, G. C. (2014). Rare earth doped glasses for displays and light generation. Advances in Science and Technology, 90, 174-178.
5. Devi, S. (2021). Asymmetric Tsallis distributions for modeling financial market dynamics. Physica A: Statistical Mechanics and Its Applications, 578, 126109
6. El Mendili, Y. (2017). Raman spectrum of commercial Eu2O3. Personal communication to ROD, https://solsa.crystallography.net/rod/3500047.html
7. El Mendili, Y. (2017). Raman spectrum of commercial holmium(III) oxide. Personal communication to ROD, https://solsa.crystallography.net/rod/3500009.html
8. El Mendili, Y. (2017). Raman spectrum of commercial erbium(III) oxide, Personal communication to ROD, https://solsa.crystallography.net/rod/3500007.rod
9. El Mendili, Y. (2017). Raman spectrum of commercial Nd2O3, Personal communication to ROD, 2017, https://solsa.crystallography.net/rod/3500066.rod
10. El Mendili, Y. (2017). Raman spectrum of commercial Samarium (III) oxide. Personal communication to ROD, 2017, https://solsa.crystallography.net/rod/3500097.rod
11. El Mendili, Y., Vaitkus, A., Merkys, A., Gražulis, S., Chateigner, D., Mathevet, F., Gascoin, S., Petit, S., Bardeau, J.F., Zanatta, M., & Secchi, M. (2019). Raman Open Database: first interconnected Raman–X-ray diffraction open-access resource for material identification. Journal of applied crystallography, 52(3), pp.618-625.
12. Fang, J., Sun, L., Guo, S., Liu, C., & Zhang, J. (2021). Study of Li2O addition on crystallization behavior and thermal expansion properties of CaO-Al2O3–SiO2 (CAS) glass-ceramic and its application for joining SiC ceramic. Journal of the European Ceramic Society, 41(3), 1817-1827.
13. Ferrari, A. C., & Robertson, J. (2000). Interpretation of Raman spectra of disordered and amorphous carbon. Physical Review B 61: 14095–14107.
14. Geissinger, P., Giering, T., Richter, W., & Haarer, D. (2000). Doped Rare Gas Solids as Model Systems for Chromophore−Matrix Interactions. Accounts of Chemical Research, 33(3), 131-138.
15. Hanel, R., Thurner, S., & Tsallis, C. (2009). Limit distributions of scale-invariant probabilistic models of correlated random variables with the q-Gaussian as an explicit example. The European Physical Journal B, 72(2), 263.
16. Kumar, A., Rai, D. K., & Rai, S. B. (2002). Optical studies of Eu3+ ions doped in tellurite glass. Spectrochimica Acta Part A: Molecular and Biomolecular Spectroscopy, 58(10), 2115-2125.
17. Lafuente, B., Downs, R. T., Yang, H., & Stone, N. (2015). 1. The power of databases: The RRUFF project. In Highlights in mineralogical crystallography (pp. 1-30). De Gruyter (O).
18. Locardi, B., & Guadagnino, E. (1992). Rare earths in glass technology. Materials chemistry and physics, 31(1-2), 45-49.
19. Malba, C.M., Enrichi, F., Facchin, M., Demitri, N., Plaisier, J.R., Natile, M.M., Selva, M., Riello, P., Perosa, A., & Benedetti, A. (2015). Phosphonium-based tetrakis dibenzoylmethane Eu (III) and Sm (III) complexes: synthesis, crystal structure and photoluminescence properties in a weakly coordinating phosphonium ionic liquid. RSC Advances, 5(75), pp.60898-60907.
20. Meltzer, R. S. (2005). Line broadening mechanisms and their measurement. In Spectroscopic properties of rare earths in optical materials (pp. 191-265). Berlin, Heidelberg: Springer Berlin Heidelberg.
21. Miniscalco, W. J. (2001). Optical and electronic properties of rare earth ions in glasses. Optical Engineering, Marcel Dekker Incorporated, 71, 17-112.
22. Miroshnichenko, A. E., Flach, S., & Kivshar, Y. S. (2010). Fano resonances in nanoscale structures. Reviews of Modern Physics, 82(3), 2257.
23. Mo-Sci. (2023, June 02). Using Rare Earth Oxides to Make Fluorescent Glasses. AZoM. Retrieved on July 15, 2024 from https://www.azom.com/article.aspx?ArticleID=18870.
24. Naudts, J. (2009). The q-exponential family in statistical physics. Central European Journal of Physics, 7, 405-413.

25. Roth, R. S., & Schneider, S. J. (1960). Phase equilibria in systems involving the rare-earth oxides. Part I. Polymorphism of the oxides of the trivalent rare-earth ions. Journal of Research of the National Bureau of Standards. Section A, Physics and Chemistry, 64(4), 309.

26. Sadagov, A. Y., Goidina, T. A., Aseev, V. A., Nikonorov, N. V., Fedorov, Y. K., Chugunova, M. M., & Levin, A. D. (2020). Spectral standards based on glasses activated with rare-earth element ions for the calibration of fluorescence and Raman spectrometers. Optics and spectroscopy, 128, 1658-1666.

27. Shelby, J. E. (1985). Formation and properties of calcium aluminosilicate glasses. Journal of the American Ceramic Society, 68(3), 155-158.

28. Sidebottom, D. L., Hruschka, M. A., Potter, B. G., & Brow, R. K. (1997). Structure and optical properties of rare earth-doped zinc oxyhalide tellurite glasses. Journal of non-crystalline solids, 222, 282-289.

29. Sparavigna, A. C. (2023). q-Gaussian Tsallis Line Shapes and Raman Spectral Bands. Int. J. Sciences, 12(3), 27-40, 2023, http://dx.doi.org/10.18483/ijSci.2671 Available at SSRN: https://ssrn.com/abstract=4398623

30. Sparavigna, A. C. (2023). Asymmetric q-Gaussian functions generalizing the Breit-Wigner-Fano functions. Zenodo. https://doi.org/10.5281/zenodo.8356165

31. Sparavigna, A. C. (2023). SERS Spectral Bands of L-Cysteine, Cysteamine and Homocysteine Fitted by Tsallis q-Gaussian Functions. International Journal of Sciences, 12(09), 14-24.

32. Sparavigna, A. C. (2023). q-Gaussian Tsallis Line Shapes for Raman Spectroscopy (June 7, 2023). SSRN Electronic Journal. http://dx.doi.org/10.2139/ssrn.4445044

33. Sparavigna A. C. (2023). Tsallis q-Gaussian function as fitting lineshape for Graphite Raman bands. ChemRxiv. Cambridge: Cambridge Open Engage; 2023.

34. Sparavigna, A. C. (2024). Kubo Lineshape and its Fitted q-Gaussian Tsallis Function. International Journal of Sciences, 13(01), 1-9.

35. Sparavigna, A. C. (2024). The Fitted q-Gaussian Function, from Voigt Profile to Kubo Lineshape. International Journal of Sciences, 13(03), 1-16.

36. Sparavigna, A. C. (2024). Applying q-Gaussians to the OH- stretching Raman bands of Water and Ice. International Journal of Sciences, 13(04), 1-10.

37. Sparavigna, A. C. (2024). Molybdenum Disulfide MoS2 and the q-BWF line shapes (Raman Spectroscopy). ChemRxiv. doi:10.26434/chemrxiv-2024-cprs3-v3 This content is a preprint and has not been peer-reviewed.

38. Tokmakoff, A. (2014). Time-Dependent Quantum Mechanics and Spectroscopy. University of Chicago. 2014. Available online: https://tdqms.uchicago.edu/#notes

39. Tsallis, C. (1988). Possible generalization of Boltzmann-Gibbs statistics. Journal of statistical physics, 52, 479-487.

40. Tuschel, D. (2016). Photoluminescence Spectroscopy Using a Raman Spectrometer. Spectroscopy, 31 (9),14–21

41. Umarov, S., Tsallis, C., Steinberg, S. (2008). On a q-Central Limit Theorem Consistent with Nonextensive Statistical Mechanics. Milan J. Math. Birkhauser Verlag. 76: 307–328. doi:10.1007/s00032-008-0087-y. S2CID 55967725.

42. Wakefield, G., Holland, E., Dobson, P. J., & Hutchison, J. L. (2001). Luminescence properties of nanocrystalline Y2O3: Eu. Advanced Materials, 13(20), 1557-1560.

43. Wang, M., Xiong, Q., Wang, M., Lewis, N.H., Ying, D., Yan, G., Hoenig, E., Han, Y., Lee, O.S., Peng, G., & Zhou, H. (2024). Lanthanide transport in angstrom-scale MoS2-based two-dimensional channels. Science Advances, 10(11), p.eadh1330.

44. Wojdyr, M. (2010). Fityk: a general-purpose peak fitting program. Journal of applied crystallography, 43(5), 1126-1128.

45. Xin, R. F., & Guo, X. M. (2022). A Study of the Crystallization Properties of CaO-SiO2-Al2O3 Glass Phase in Sinter. Metals, 12(6), 915.

46. Yu, J., Cui, L., He, H., Yan, S., Hu, Y., & Wu, H. (2014). Raman spectra of RE2O3 (RE= Eu, Gd, Dy, Ho, Er, Tm, Yb, Lu, Sc and Y): laser-excited luminescence and trace impurity analysis. Journal of rare earths, 32(1), 1-4.

47. Zhang, H., & Zhang, H. (2022). Rare earth luminescent materials. Light: Science & Applications, 11(1), 260.

48. Zhao, Z., Shi, J., Sun, Z., Lin, J., Huang, W., & Wang, Z. (2004). Nonlinear optical properties of Eu2O3 doped 5ZnO-20Nb2O5-75TeO2 glasses. Chinese Science Bulletin, 49, 2446-2448.